Development of bioanodes rich in exoelectrogenic bacteria using iron-rich palaeomarine sediment inoculum

Fatima-Zahra Ait-Itto, James Behan, Mathieu Martinez, Frédéric Barrière

Development of bioanodes rich in exoelectrogenic bacteria using iron-rich palaeomarine sediment inoculum

Fatima-Zahra Ait-Itto [a,b], James A. Behan [a], Mathieu Martinez [b], Frédéric Barrière [a*]

[a] *Université de Rennes, CNRS, Institut des Sciences Chimiques de Rennes, UMR 6226, Rennes, France*

[b] *Université de Rennes, CNRS, Géosciences de Rennes – UMR 6118, Rennes, France*

**Corresponding author:* frederic.barriere@univ-rennes.fr

Abstract

Microbial Fuel Cells (MFC) convert energy stored in chemicals into electrical energy thanks to exoelectrogenic microorganisms who also play a crucial role in geochemical cycles in their natural environment, including that of iron. In this study, we investigated paleomarine sediments as inoculum for bioanode development in MFCs. These sediments were formed under anoxic conditions ca. 113 million years ago and are rich in clay minerals, organic matter, and iron. The marlstone inoculum was incubated in the anolyte of an MFC using acetate as the added electron donor and ferricyanide as the electron acceptor in the catholyte. After seven weeks of incubation, the current density increased to 0.15 $mA.cm^{-2}$ and a stable +700 mV open circuit potential was reached. Community analysis revealed the presence of two exoelectrogenic bacterial genera, *Geovibrio* and *Geobacter*. Development of electroactive biofilms was correlated to bulk chemical transformations of the sediment inoculum with an increase in the Fe(II) to Fe_{total} ratio. Comparisons to sediments sterilized prior to inoculation confirmed that bioanode development derives from the native microbiota of these paleomarine sediments. This study illustrates the feasibility of developing exoelectrogenic biofilms from iron-rich marlstone and has implications for the role of such bacteria in broader paleoenvironmental phenomena.

Keywords:

Exoelectrogenic bacteria, biofilms, bio-anode, paleomarine sediments, clay minerals

Introduction

The process of Fe (III) reduction by exoelectrogenic bacteria is crucial in the iron geochemistry cycle and plays a vital role in the degradation of natural and contaminant/waste organic compounds [1–3]. Exoelectrogenic bacteria have potential applications in the fields of bioremediation and biotechnology, as they can oxidize organic contaminants such as aromatic hydrocarbons anaerobically in anoxic petroleum-contaminated aquifers and simultaneously reduce Fe (III) [4]. For example, one study suggests that exoelectrogenic bacteria also play a fundamental role in Precambrian banded iron formations, as evidenced by the strong correlation between isotopically-light carbonates and iron minerals accumulations that occurred through a combination of organic matter mineralization and Fe (III) reduction [5]. Thus, much research has been conducted to better understand the interaction between microorganisms and sediments in different environments, as this relationship plays a role in biogeochemical cycles where bacteria can alter the physical and chemical state of sediments [6]. Marine sediments are well-known as a source of abundant electrochemically active bacteria [7] and have been used as inoculum in sediment Microbial Fuel Cells (MFCs) for simultaneous energy production and bioremediation [8]. It is essential to highlight that the amount of energy obtained in the MFCs devices depends on several factors, including the quantity of organic matter and type of exoelectrogenic microorganisms present in the sediments [9,10]. Moreover, it can be argued more broadly that climatological factors and geological conditions play a role in MFC development, by influencing the microbiota composition of natural inoculum. In this context, the exploration of paleomarine sediments from a geological perspective offers a promising avenue for pinpointing actual and past environments conducive to the development of microorganisms, and selecting appropriate sediments for inoculation of MFCs [11].

In this study, we focus on the development of electroactive biofilms using paleomarine sediment inoculum formed in hemipelagic environment, characterized by a large deposition of organic-rich layers with accumulation of weathering products [12]. These ancient geological deposits are rich in clay minerals, including smectite, illite, kaolinite and chlorite, but also showcase high iron contents (primarily Fe(III)) as well as organic matter. These conditions may provide a favorable environment for the development of electroactive bacteria. Herein we demonstrate the development of acetate-metabolizing bioanodes in a microbial fuel cell system using these iron-rich paleomarine sediments as the inoculum. Physico-chemical

characterization of the sediments in the anolyte after continuous operation shows a distinct increase in the proportion of Fe(II) oxides to the total iron oxide content ($Fe(II)/Fe_{total}$) consistent with the presence of exo-electrogens utilizing abundant Fe(III) in the sediments as the sole electron acceptor under anaerobic conditions. Using 16S rRNA amplicon sequencing we correlate these changes in sediment composition to the development of mixed biofilms containing *Pelobacter* genus and some well-known exo-electrogens species from the genera *Geovibrio* and *Geobacter*.

2. Materials and methods

2.1 Sample collection

The Paleomarine Sedimentary rock (PS) used in this study are marlstone (mixture between clay and calcite), with organic matter content around 1.3 %. The samples were collected from Col de Pré-Guittard section of the Vocontian basin in France, located approximately at 11 km north-northwest of Rémuzat, Drôme (Supporting Information Figure S1). The clay mineral assemblages of the Col de Pré-Guittard section consist mainly of smectite (averaging 63%), illite (averaging 19%), and kaolinite (averaging 11%), along with approximately 5% chlorite [13]. The selected marlstone sample was crushed into powder using an agate mortar to achieve an average particle size < 125 μm. X-ray diffractometry (XRD) was employed to identify the mineral phases present in the sediment, revealing the presence of quartz, calcite, gypsum, and clay minerals (Supporting Information Figure S2). The Scanning electron microscopy (SEM) image of the PS revealed a platy-shaped structure of clay mineral particles. The elemental composition of PS recorded the presence of high levels of alumino-silicate (approximately 20% of Si and 8% of Al) arising from the clay, as well as a significant quantity of Fe element, approximately 5.8% (Supporting Information Figure S2).

2.2 Chemical reagents

Potassium acetate (> 99%, anhydrous), glutaraldehyde (25% solution), potassium hexacyanoferrate III ($K_3Fe(CN)_6$), potassium phosphate dibasic (K_2HPO_4), and potassium phosphate monobasic (KH_2PO_4) were purchased from Sigma Aldrich and used without further purification.

2.3 Bio-anode Setup & electrochemical measurements

The marlstone samples were incubated under anoxic conditions that are favorable for the development of exoelectrogenic bacteria as previously reported [14] [15]. Briefly, an H-type reactor was used with 250 mL compartments separated by a Cation Exchange Membrane

(Fumasep® FKM). Graphite rods (Morgan AM&T) with a diameter of 0.5 cm and height of 20 cm were used as electrodes in both compartments. For the anodic compartment, the electrode was cleaned using pure water in ultrasound for 10 min, then covered by parafilm to fix the surface at 4.9 cm^2. In the anodic compartment, 8.05 g of marlstone samples was mixed with 250 mL of phosphate buffer (10 mM) prepared using ultrapure (18.2 MΩ.cm) water. The chosen concentration is consistent with the previous experiments using low ionic strength electrolytes which successfully developed bioanodes from mixed inoculum[16] The pH of the anodic compartment was measured and adjusted to pH 7 using 2M NaOH. Potassium acetate (10 mM) was regularly added as an electron donor from filtered anoxic stock solutions.

The cathodic compartment was filled with 250 mL of phosphate buffer (10 mM) containing potassium hexacyanoferrate (50 mM) as an electron acceptor. The cathode showed a stable potential (*ca.* 0.2 V vs Ag/AgCl 3 M KCl) which remained constant throughout the experiment. The two compartments were connected by an external resistor 1-4 kΩ to match the internal resistance of the MFC as determined via impedance spectroscopy measurements using a Multi Autolab / M204 potentiostat [15]. These pilots are designated as PS/MFC (PS/MFC 1 and PS/MFC 2).

A control cell (PS/Control) was also established and incubated under identical conditions without connection to an external cathode designated as (PS/Ctrl 1 and PS/Ctrl 2). To maintain the MFC under anaerobic conditions, the anodic compartment was purged with argon gas for 30 minutes once every 5 days on average. MFCs were incubated in the dark at 30 °C in a thermostatic bath (Supporting Information Figure S3). The open circuit potential (OCP) between the electrodes was measured periodically using a digital multimeter or potentiostat. MFCs were left at open circuit for at least 30 minutes prior to taking the measurement. To monitor the development of exo-electrogenic bacteria from the marlstone samples, the bio-anode was regularly studied using cyclic voltammetry in the range -0.8 to +0.4 V vs Ag/AgCl 3 M KCl at a scan rate of 2 mV/s unless otherwise specified. Electrochemical measurements were performed using a three-electrode set-up where the bioanode served as the working electrode, Ag/AgCl (3 M KCl) as the reference electrode placed in the anolyte, and the cathode (graphite rod) was used as a counter electrode. All experiments were conducted in duplicate under an inert atmosphere using Ar saturation. Samples of solution or sediments from the MFCs were taken under argon flux with sterile syringes to minimize disturbance to the bioanodes and preserve anaerobic conditions. Additional control experiments were

performed using sterilized inoculum: the paleomarine sediments were dispersed in a small volume of ultrapure water and autoclaved (Autoclave Steril Elite^{TM}, Fisher Scientific brand) for 1 hour at 121°C and then incubated under identical conditions to the PS/MFC.

2.4. X-Ray Photoelectron Spectroscopy (XPS)

In all cases, powder samples for XPS analysis were prepared by pressing the powder (0.1 g) on carbon tape mounted on the conductive sample holder. XPS data were obtained using a NEXSA G2 (ThermoFischer Scientific) spectrometer using an Al Kα X-ray source working at 1486.6 eV with a spot size of 200 µm². Survey spectra (0-1000 eV) were acquired with an analyzer pass energy of 200 eV (1 eV/step); high-resolution spectra used a pass energy of 50 eV (0.1 eV/step). Charge compensation using a flood gun was applied to all powder preparations and the binding energies corrected to the position of the C 1s peak assigned to adventitious carbon at 284.8 eV. Spectra were peak-fitted using commercial software (CasaXPS Version 2.3.18). Deconvolutions were performed using Shirley background subtraction in all cases. Peak areas used in quantitative analysis were normalized by relative sensitivity factors for atomic percentage determination (C 1s = 1, O 1s = 2.93, Si 2p= 0.817, Ca 2p = 5.07, Fe 2p = 16.42, K 2p = 3.97, Mg 2s = 0.575, P 2p = 0.817, Na 1s = 8.52, Al 2p = 0.537).

2.5. X-Ray Diffraction (XRD)

To determine the mineral phases, present in the marlstone samples, X-Ray Diffraction (XRD) was conducted. Dry powder samples were analyzed using a Bruker D8 Endeavour diffractometer equipped with CuKa radiations, a LynxEye_XE_T detector, and a Ni filter. The instrument was set at a voltage of 40 kV and an intensity of 25 mA. The goniometer scanning ranged from 2° to 65° for each analysis. The identification of mineral phases was accomplished by analyzing their primary diffraction peak (d001).

2.6. Scanning Electron Microscopy imaging (SEM) and Inductively Coupled Plasma Mass Spectroscopy (ICP-MS)

SEM samples were prepared following the protocol of reference [17]. First, the samples are fixed overnight with 2.5% glutaraldehyde in buffer phosphate solution (0.1 M, pH 7) at room temperature. Then, samples were washed using a phosphate buffer solution (pH 7) and immersed respectively in an aqueous solution containing increasing ethanol concentrations from 50%-100% as previously reported [15]. Finally, the samples were critical-point dried to

157 replace the remaining water and ethanol solvent with CO_2 and Au-coated. The analysis was
158 performed using a JEOL JSM 7100 F EDS EBSD Oxford Scanning Electron Microscope.
159 To estimate the overall concentration of oxides and total iron content, we used an ICP-MS
160 (Inductively Coupled Plasma-Mass Spectroscopy) iCapQ ThermoFisher performed by the
161 National Service of Rocks and Minerals Analysis (SARM: http://helium.crpg.cnrs-
162 nancy.fr/SARM/) in Nancy. Prior to the analysis, it is necessary to prepare the samples through
163 alkaline fusions using lithium metaborate ($LiBO_2$). Fe(II) content was established using
164 potentiometric titration for calculations of the ratio $Fe(II)/Fe_{total}$.
165

2.7. DNA extraction from the biofilm

After the incubation and development of the biofilm, DNA extraction was performed on all samples using the DNeasy PowerSoil DNA extraction kit (Qiagen®) according to the manufacturer's protocol. Prior to DNA extraction the biofilm developed on the surface of the electrode was gently scraped using a spatula sterilized with absolute ethanol. To investigate the distribution of bacterial communities throughout the entire anodic compartment, DNA was also extracted from the solution-sediment interface. The concentration of DNA was verified using a Nanodrop® and all samples reported had sufficient DNA to proceed with sequencing. The 16S rRNA gene sequencing was done by the GeT-Biopuces laboratory at INSA Toulouse. The variable region V4-V5 of the 16S rRNA was targeted using the primers 515F (5'-GTGCCAGCMGCCGCGGTAA-3') and 928R (5'-CCCCGYCAATTCMTTTRAGT-3'). The amplified products were then sequenced using an Illumina MiSeq instrument, and the results were obtained in the FastQ format [15].

3. Results

3.1. Characterization of the bioanode developed at the surface of the electrode

During the initial days of incubation, the Open Circuit Potential (OCP) was 200 mV (Figure 1a) versus the cathode which held a constant potential of 0.2 V vs Ag/AgCl (3 M KCl) throughout the experiment, maintained using 50mM of potassium hexacyanoferrate (III) as an electrolyte in the cathodic compartment [18]. Cyclic voltammograms showed a typical graphite background with only capacitive current (Figure 1b, black curve). After 14 days of incubation, the OCP of PS/MFC pilots significantly increased up to a maximum of *ca*. 700 mV and remained stable upon periodic measurement thereafter. This OCP increase is attributed to the development of an electroactive biofilm capable of acetate oxidation at the surface of the graphite rod. This is confirmed in cyclic voltammetry studies of the mature bioanodes (Figure 1b, red curve) developed in PS/MFC1 which shows a sigmoidal oxidation curve with onset between -0.6 and -0.5 V vs Ag/AgCl 3 M KCl attributed to catalytic acetate oxidation. Additional redox peaks centered between -0.42 to -0.30 V are attributed to outer membrane cytochromes present in the electroactive biofilm [19], [15]. A further oxidation peak was observed between -0.2 V and-0.18 V vs Ag/AgCl 3 M KCl consistent with the presence of iron oxides surrounding the biofilm as previously reported [15].

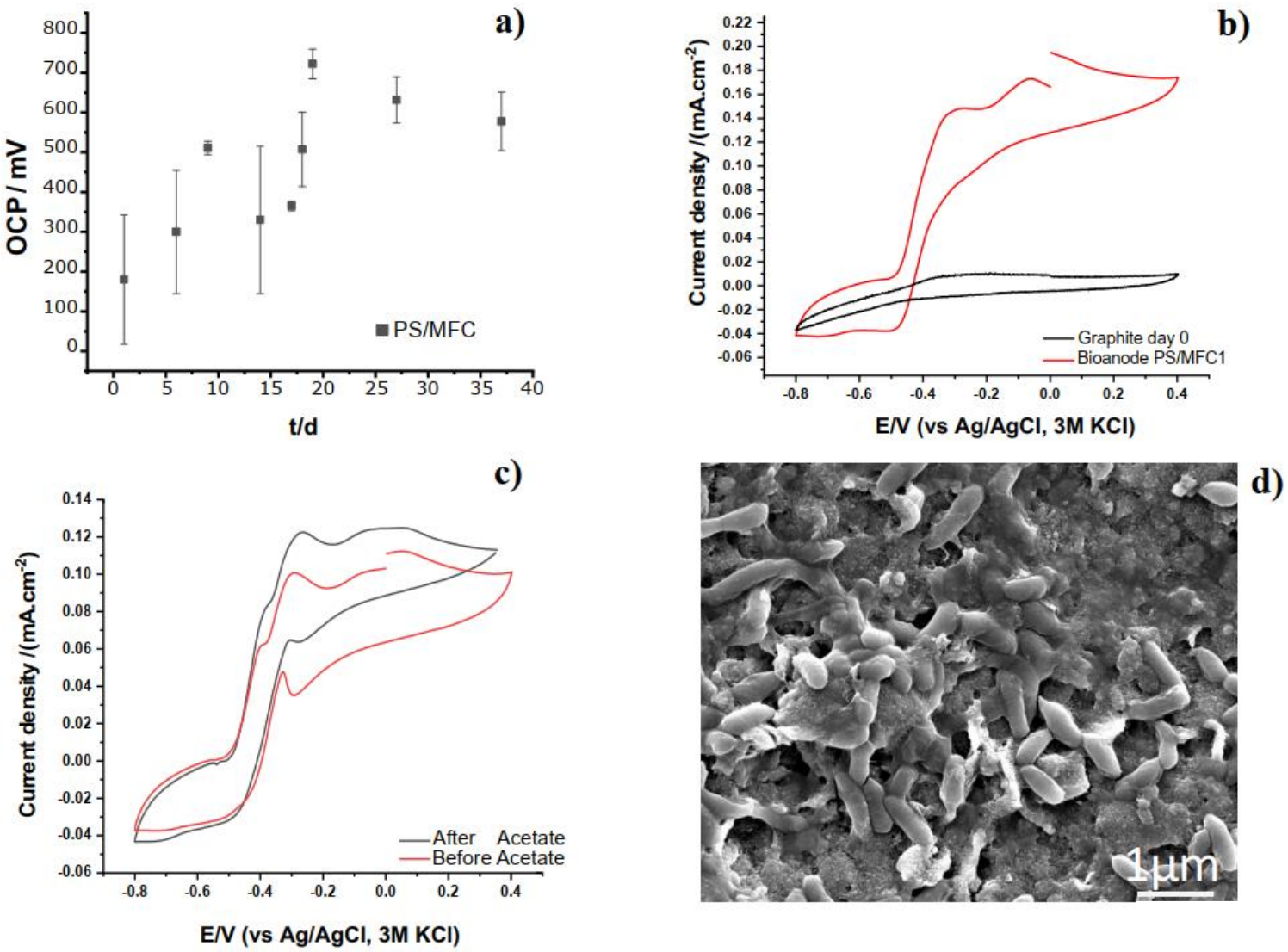

198

199 **Figure 1.** a) Open circuit potential (OCP) of both PS/MFC Pilots (MFC1 and MFC2) obtained after 40
200 incubation days. b) Cyclic voltammogram recorded from the PS/MFC1 pilot from the first day of
201 incubation (black curve) and again after 90 days of incubation (red curve). c) Cyclic voltammograms of
202 bioanode PS/MFC1 before and after the addition of 10 mM acetate. d) SEM image of a mature mixed
203 bioanode developed from PS/MFC1.

At this point, such biofilms yielded reproductible voltammograms with the sigmoidal catalytic profile, in both pilots (PS/MFC1 and PS/MFC2; see supporting information Figure S4b) compared to the sterilized pilots that show no catalytic profile (see supporting information Figures S5, S6b) with an OCP around 400 mV compared to the PS/MFC that recorded 700 mV at the same period of incubation (see supporting information Figure S6a). The specificity of the acetate response was confirmed by an enhancement in the catalytic current upon re-addition of 10 mM acetate after 24h of constant turnover in PS/MFC1 (Figure 1c). The acetate dependence was also replicated on other independent pilots (see supporting information Figure S4a). These results suggest that the exoelectrogenic bacteria developed at the bioanode in PS/MFC pilots provided from the initial paleomarine inoculum. Moreover, a complete loss of catalytic activity was observed after the removal of the biofilm for DNA extraction (Supporting Information Figure S7), thus confirming that the catalytic response observed could be attributed to a biofilm developed on the electrode surface (see supporting information Figure S8). SEM imaging of the bioanode after glutaraldehyde fixation confirmed the presence of a mixed bacterial biofilm at the electrode surface. A representative image is shown in Figure 1d and indicates that bacteria grow across the graphite surface (Supporting Information Figure S9a). The control electrode which was not electrically coupled to a cathode through a resistor also shows significant biomass but not a continuous biofilm as same form as anodes operated as MFCs (Supporting Information Figure S9b-d and S10). This result is consistent with community analysis from 16S as discussed below.

3.2. Extraction of the biofilm and community determination

Based on electrochemical experiments and SEM images, it is evident that a mixed community electroactive biofilm has developed on the surface of the graphite electrode. To enhance electron transfer efficiency and gain a better understanding of the electron transfer mechanism, it is crucial to identify and study the physiology of anodic microbial communities developed on the electrode surface, as this serves as a fundamental aspect in optimizing electron transfer processes and improving overall system performance [7].

To determine the nature of the biofilm colonizing the bioanode, 16S amplicon sequencing analysis was conducted on the PS/MFC pilots, SPS/MFC pilots, controls, and PS day 0. The sequencing analysis for all the pilots revealed the abundance of three phyla Proteobacteria, Firmicutes, and Bacteroidetes (Figure 2). These findings align with the initial composition of the marlstone samples before incubation (see Supporting Information Figure S11). Notably, we recorded the growth of Deferribacteres phylum at the PS/MFC (PS/MFC 2) with a relative abundance of around 10 %. This phylum was initially present in the marlstone samples prior to incubation with a low abundance of less than 0.1% and developed under the incubation conditions to reach 10%. The growth of this phylum suggests the development of exoelectrogenic bacteria at the anodic compartment such as those of the *Geovibrio* genus, capable of reducing metal ions. This genus has been found to have industrial applications, including the conversion of organic compounds to biofuels [20].

These results are not surprising, knowing that the Proteobacteria are the most abundant phylum in soil [21], which includes important exoelectrogenic bacteria such as those of the *Geobacter* genus, able to oxidize organic compounds completely to carbon dioxide with an anode serving as the sole electron acceptor [22] [23]. Likewise, in the Firmicutes phylum, some isolated members can transfer electrons to solid phases as electron acceptors [24], including iron and manganese, as part of a respiratory mechanism [25]. Bacteroidetes phylum has been associated with the anodic biofilm and reported as a fermentative phylum able to hydrolyze complex organics molecules like cellulose[26].

253

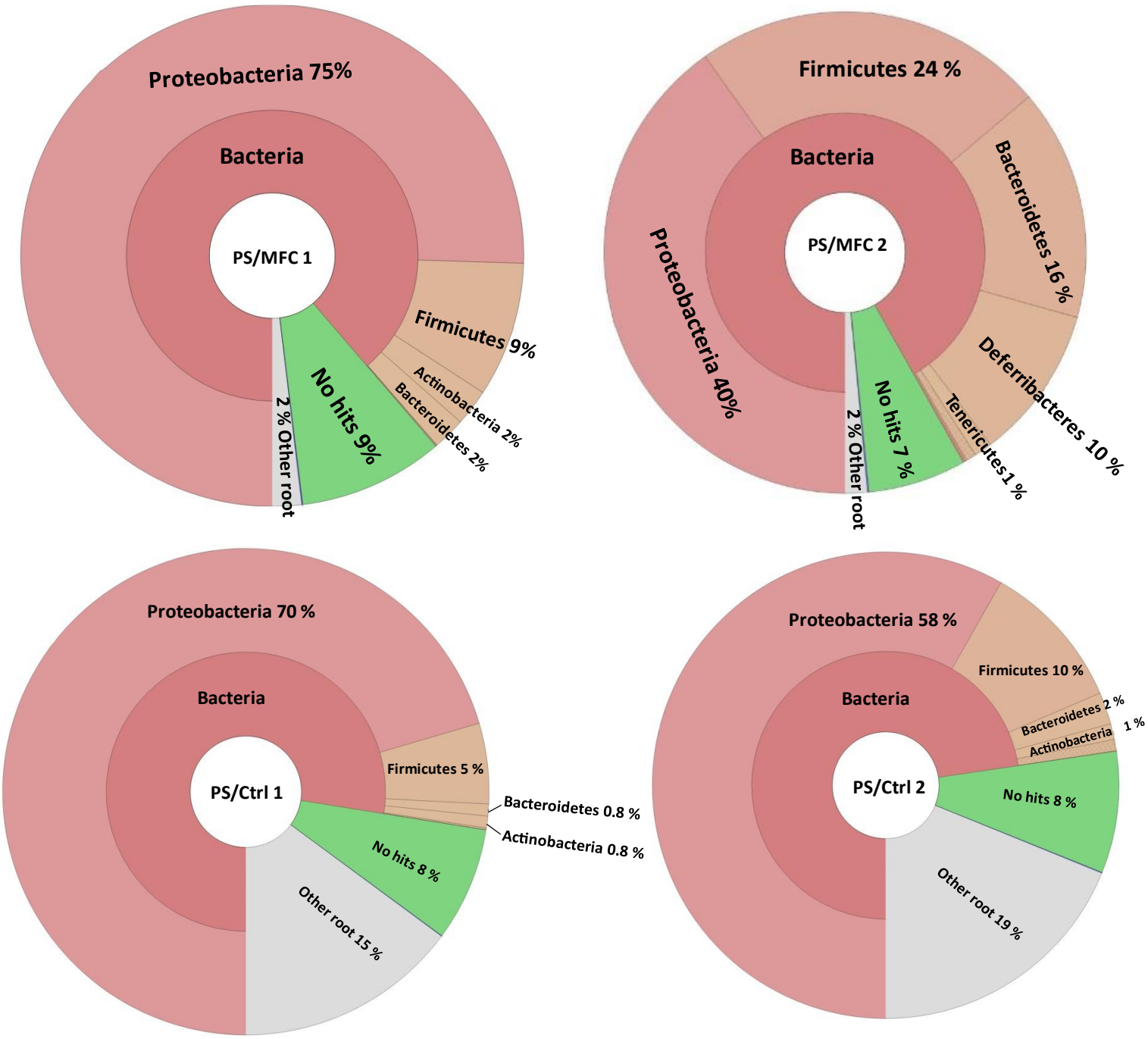

254 **Figure 2**: Relative abundance of bacterial communities (at the Phylum level) colonizing the electrode
255 from PS/MFC bioanodes (PS/MFC1 and PS/MFC 2) and from PS/Control (PS/Ctrl 1 and PS/Ctrl 2).
256

In more detailed sequencing data, we recorded the abundance of the *Pelobacter* genus in both PS/MFC duplicates, constituting approximately 33% and 25% of the microbial community recorded respectively in PS/MFC 1 and PS/MFC 2 (Figure 3). The abundance of *Pelobacter* at the anode surface is not surprising as *Pelobacter* is often isolated from anodic biofilms [27] including a recent study from our group [15]. In general, bacteria of the *Pelobacter* genus are not able to oxidize acetate and perform extracellular electron transfer simultaneously. While recent studies recorded the presence of some species of *Pelobacter* (*Pelobacter carbinolicus*) able to reduce Fe(III) and S(0) by an incomplete oxidation of organic substrates[28], they typically reduce smaller quantities of Fe(III) compared to *Geobacter* and *Desulfuromonas* species [29]. Indeed, *Pelobacter carbinolicus* is not capable of direct electron transfer to graphite anodes [30]. However, a recent publication in our team highlighted the presence of unidentified species of *Pelobacter* able to colonize the electrode and apparently transfer their electrons to the electrode directly [15]. Moreover, we registered the presence of two well-known exoelectrogenic bacterial genera, *Geobacter*, and *Geovibrio* with relative abundances of approximately 10% and 2% respectively, in PS/MFC 1 and PS/MFC 2. Previous studies have documented the occurrence of these genera in the anodic compartment, as they possess the ability to metabolize acetate and directly transfer electrons to insoluble electron acceptors [25]. Considering the low abundance (less than 1%) of the three genera in the initial sediment, we suggest that their development is favored through selective pressure under anaerobic conditions in the presence of acetate. We therefore attribute the observed catalytic behavior of PS/MFC pilots in acetate oxidation to the presence of a mixed biofilm rich in these known electricigens developed from a natural paleomarine sediment inoculum.

Considering the sequencing analysis, the presence of well-known exoelectrogenic bacteria in PS/MFC pilots is nonetheless relevant, as they may be implicated in anaerobic transformations of the marlstone samples. Community analysis of PS/Control (PS/Ctrl1 and PS/Ctrl 2) pilots incubated without external connection to a cathode showed radically different results to the PS/MFC pilots (Figure 2). Surprisingly, we recorded a large predominance of *Hydrogenophaga* in both PS/MFC duplicates, constituting approximately 49% and 45% of the microbial community recorded respectively in PS/Ctrl 1 and PS/Ctrl 2. According to previous studies, the *Hydrogenophaga* genus occurred often in the anodic biofilm community [31,32], developed under anaerobic conditions with suitable electron acceptors as nitrate or electrode in a Microbial Fuel Cell[32]. Moreover, *Hydrogenophaga* contains a species known as

Hydrogenophaga electricum that can develop under fixed flow of H_2 using a reactor connected to an electrolyzer to produce a stable concentration of H_2 [33]. Based on our findings and current understanding, the other bacteria observed in the PS/control samples do not possess a known capability for producing hydrogen from acetate. This leads to the hypothesis that hydrogen production may be attributed to unidentified bacteria or a symbiotic relationship between different bacteria present in the environment. Further investigations are currently underway to explore this possibility and shed more light on the mechanisms involved.

The low abundance of known exoelectrogenic bacteria at the electrode surface, can be explained by the presence of another electron acceptor used by bacteria instead of the electrode. To substantiate this hypothesis, we investigated the interface solution-sediment to explore the presence of a possible exoelectrogenic bacteria at the sediment surface. The sequencing results of the PS/MFC were surprising, indicating the abundance of *Advenella genus* (around 81% in PS/MFC1) known for their potential to degrade alkanes and diesel [34], and the development of *Azospirillum* (41% in PS/MFC 2) capable of nitrogen fixation [35] (Supporting Information Figure S12). However, we noted the absence of *Pelobacter*, *Geovibrio,* and *Geobacter* recorded previously at the surface of the bioanode, suggesting that this genus preferentially colonizes the electrode (Figure 2). In contrast, the PS/Ctrl pilots shows the abundance of the species *Hydrogenophaga* respectively around 40 % in PS/Ctrl 1 and 28% in PS/Ctrl 2 (Supporting Information Figure S13). Moreover, the sequencing data of SPS/MFC pilots developed from the sterilized inoculum shows a mixed biofilm with the absence of well-known exoelectrogenic bacteria (Supporting Information Figure S14). Suggesting that the sterilization effectively eliminated the initial bacteria present in the paleomarine sediment and we attribute the development of the exoelectrogenic bacteria to the initial paleomarine inoculum.

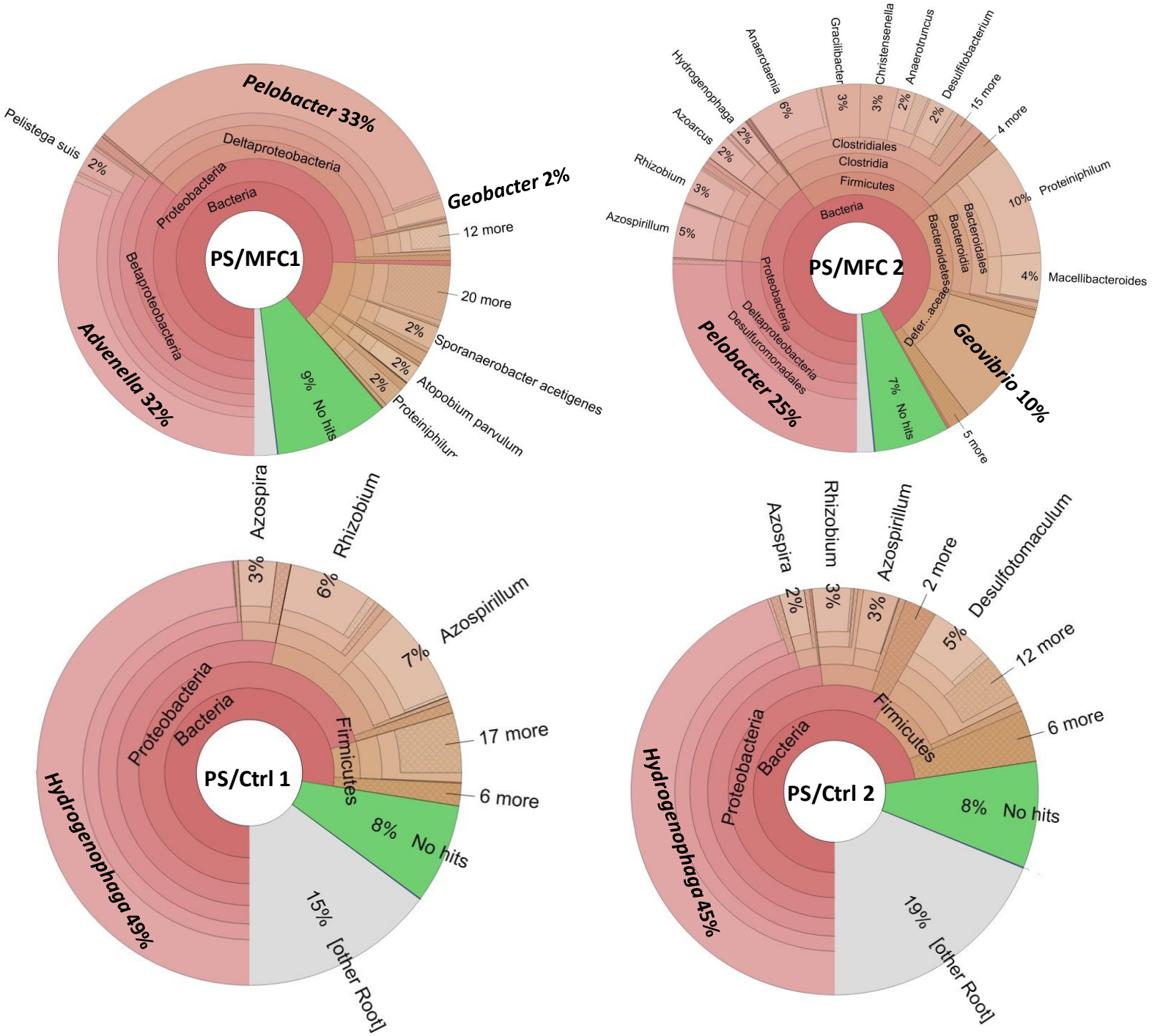

314 **Figure 3:** Summary of community analysis (species levels) colonizing the PS/MFC bioanodes,

315 PS/Control bioanodes

316

317

3.3 Bulk Chemical Changes in Sediment Samples

Under anaerobic conditions, the marlstone incubated in a microbial fuel cell (MFC) system, using acetate as an electron donor and an electrode rod as an electron acceptor, promote the growth of exoelectrogenic bacteria, as previously discussed. In addition, we observed notable environmental changes marked by the appearance of black suspended aggregate (Supporting Information Figure S15). The diffractogram analysis of the initial sediment from the marlstone sample indicated the presence of various minerals such as gypsum ($CaSO_4$), calcite ($CaCO_3$), quartz (SiO_2), and different clay minerals rich in iron like smectite, illite, kaolinite, and chlorite [13].

The X-ray diffraction performed on the black powder recovered from the PS/MFC shows the dissolution of the gypsum ($CaSO_4$, diffraction peaks G in Figure 4). Likewise, the clay mineral assemblage exhibited a broadening and shift in peak positions, indicating possible alterations in lattice parameters and crystalline structure. Additionally, the distribution of Fe in layer structure can affect the chemical reactivity of clay by affecting the layer charge which can change the properties of minerals in terms of cation exchange capacity and swelling [36] [37]. The detection of new mineral phases is difficult in our study as we used impure natural sediment without any previous treatment, which contains impurities and mixed elements (Figure 4).

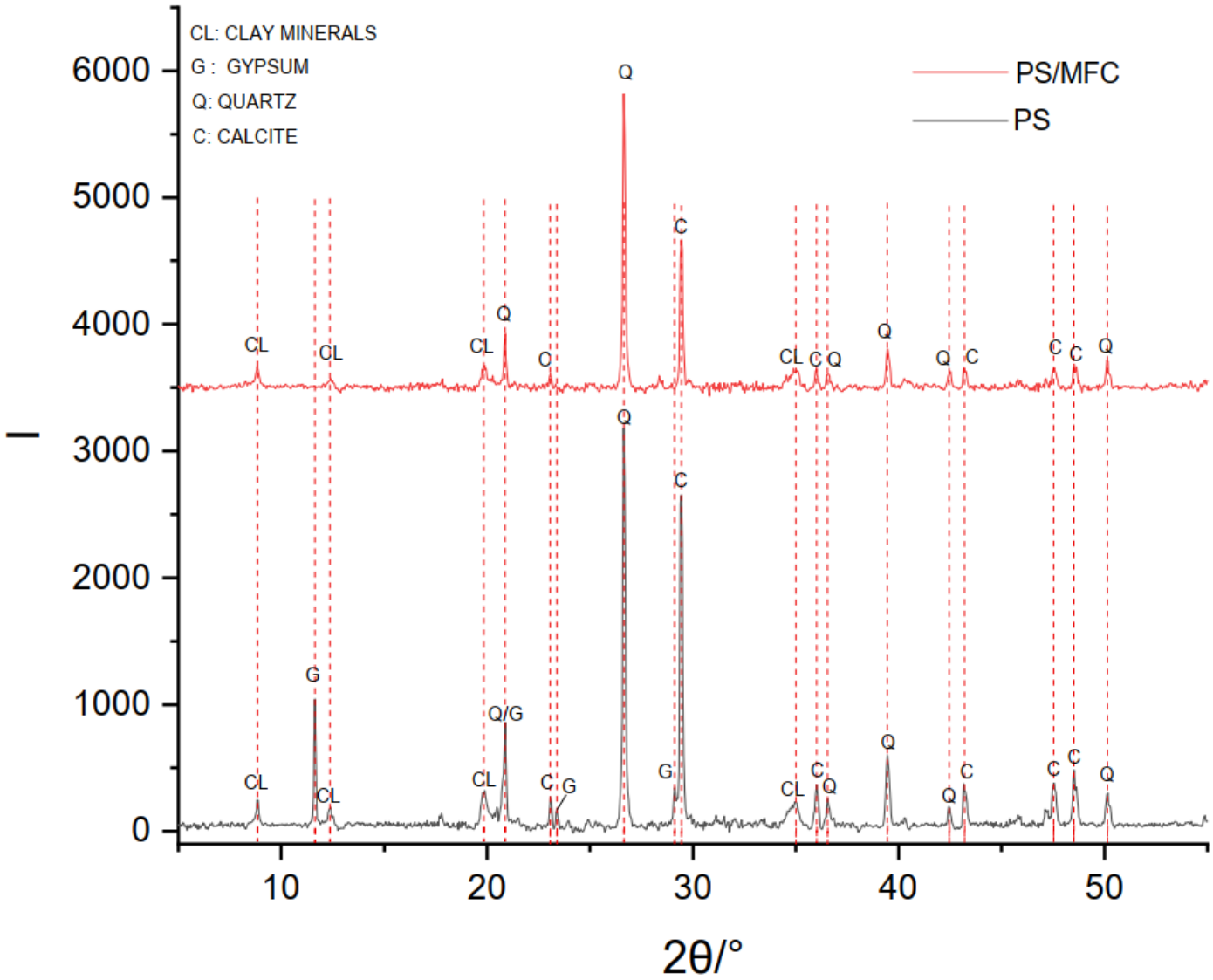

342 **Figure 4.** XRD analysis comparing the mineralogical assemblage in paleomarine sediment (PS)
343 before and after treatment (PS/MFC).
344
345 Yet, the SEM images show the presence of new precipitation rich in iron and phosphorus (from
346 phosphate buffer used as electrolyte) compared to the initial marlstone sample which is rich
347 in aluminosilicate (Figure 5, Supporting Information Figure S16). The particle size ranges of the
348 new precipitate phase and their low abundance would make this phase undetectable by XRD
349 as previously reported [38].

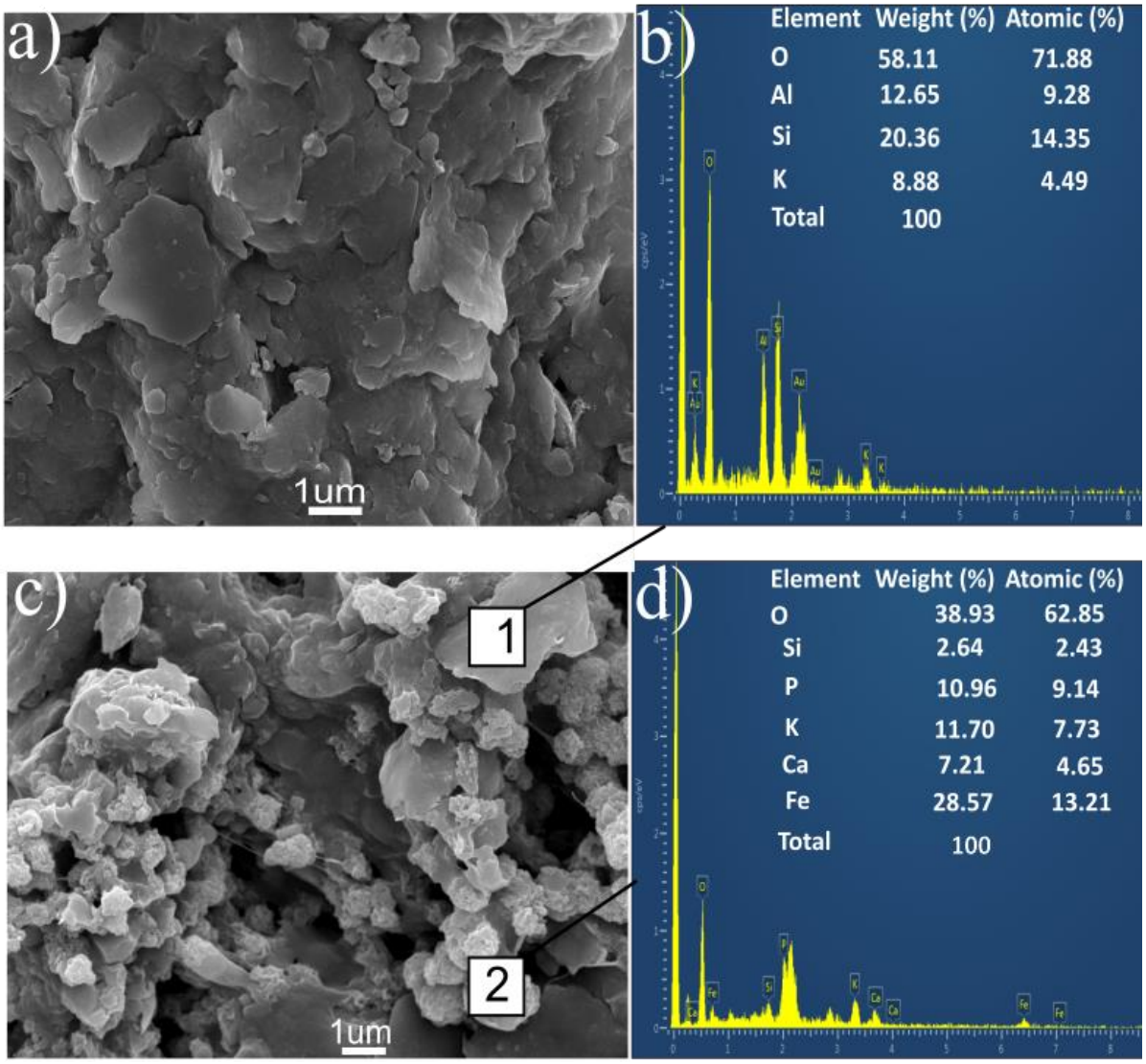

Figure 5. Scanning electron microscopy (SEM) images of the marlstones samples both before (a) and after (c) incubation (PS/MFC). a) displays the structure of clay minerals present in the PS before incubation. Small agglomerations with high concentrations of iron and potassium are observed in c) as confirmed from energy-dispersive X-ray spectroscopy (EDS) analysis (b) and d) that compares the initial composition of the PS (labeled as 1) with the composition of a new precipitate (labeled as 2). This analysis demonstrates a significant enrichment of iron in the newly formed precipitate.

These results agree with our geochemical analysis of the powder before and after incubation, where we recorded an increase on Fe_{total} and Fe (II). The potential link between the development of exoelectrogenic bacteria in the PS/MFC system and the increase in the concentration of ferrous iron Fe (II) is likely related to the reduction of Fe(III) present on the clay minerals by the developed biofilm (Figure 6) followed by re-precipitation as oxide[39]. The interaction between bacteria and clay minerals is well-known in geochemical phenomena [6]. The microorganisms have the ability to degrade and decompose clay minerals [40], promoting the conversion of smectite to illite and the biotransformation of chlorite to vermiculite [41]. Moreover, the bacteria have the ability to reduce structural iron Fe (III) of clay minerals which play a main role in iron cycles in marine sediments [42] to Fe(II) as documented for the species *Bacillus sp* isolated from clay minerals [43]. The distribution of Fe in the layered structure can affect the chemical reactivity of clay since reduction or oxidation of Fe will affect the layer charge and hence change the properties of minerals in terms of cation exchange capacity and swelling [44] [37]. According to the literature and our data, we hypothesize that the black powder developed in PS/MFC is related to the reduction of iron Fe(III) present in the marlstone samples to Fe(II) by the developed exoelectrogenic bacteria.

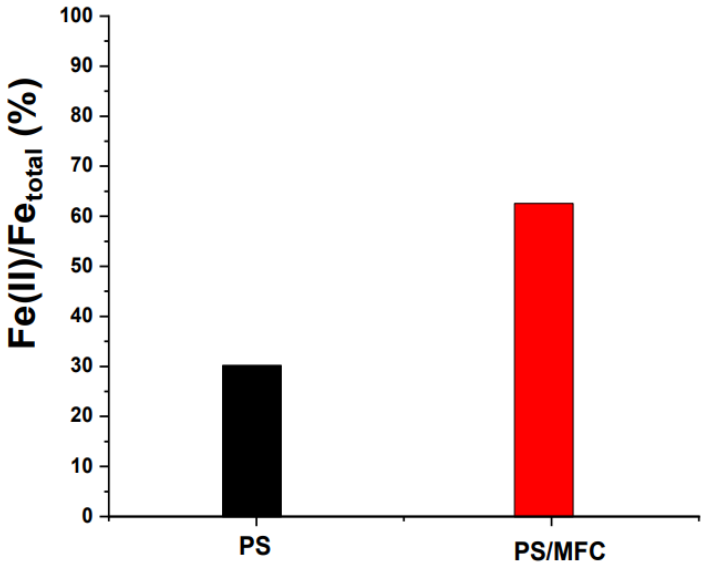

Figure 6. Iron content of the marlstone samples powder before (in black) and after incubation (in red)

After MFC operation there is an apparent increase in the contributions of potassium along with the appearance of a small phosphorus contribution in the survey, consistent with the use of potassium phosphate buffer in the electrolyte. No change in total iron content was found after MFC operation, however, changes in the oxidation state of the iron are evident in the high-resolution XPS spectra showing the Fe 2p3/2 and 2p1/2 peaks (Figure 7 b) which may be attributed to the reduction of Fe(III) to Fe(II) by electroactive bacteria.

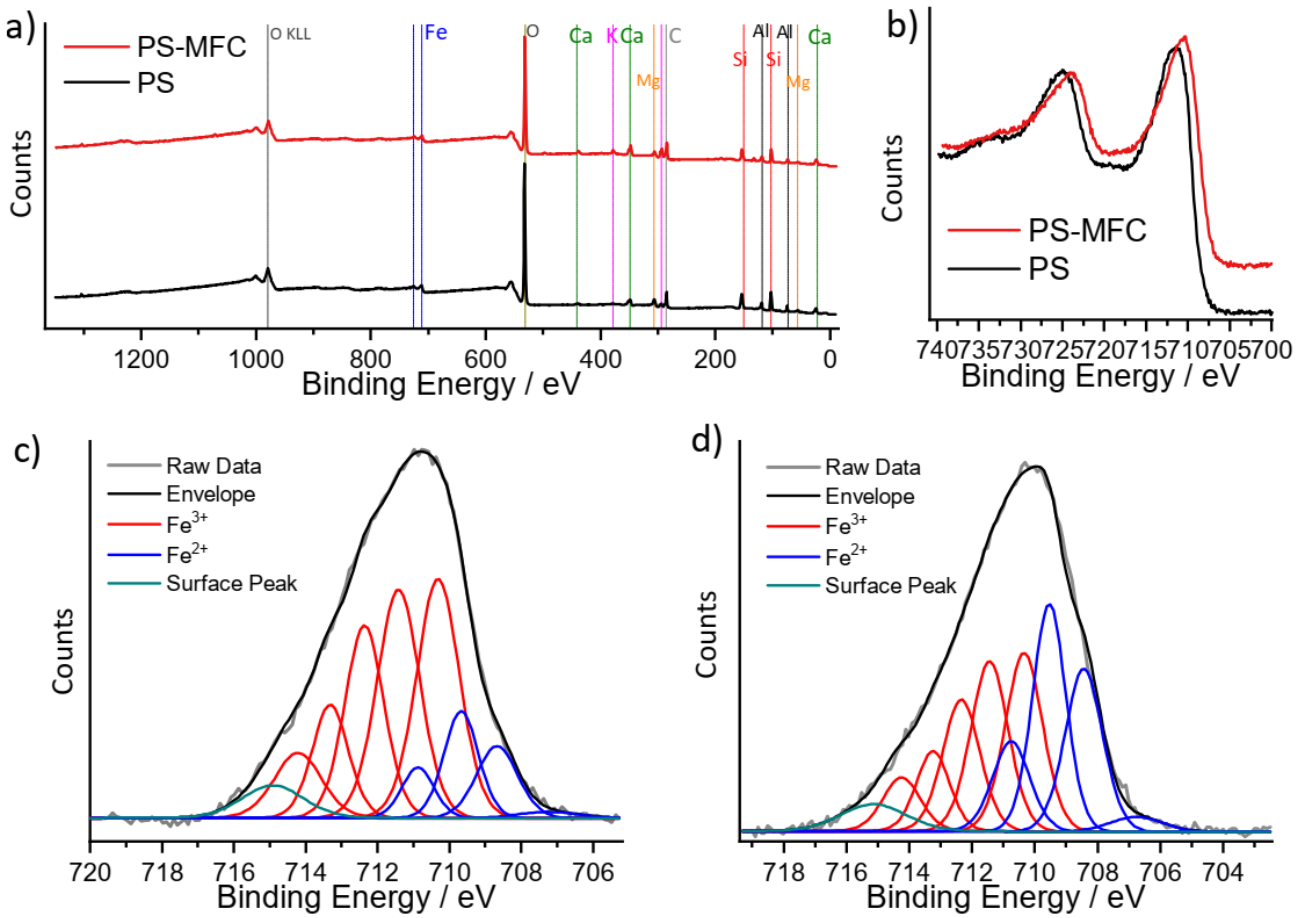

Figure 7: a) shows representative survey spectra of the PS and PS-MFC. Peaks associated to selected assigned elements are indicated above the spectra in each case. b) High resolution spectra in the region containing Fe 2p1/2 and 2p3/2 peaks after charge correction using adventitious carbon in the C 1s envelope at 284.8 eV. c) and d) show deconvoluted high resolution spectra in the Fe 2p3/2 region. Spectra are shown after Shirley background subtraction. Details of the assigned peak positions and full widths at half maximum are reported in the supporting information Table S2.

The predominant elements detected in the survey are carbon, oxygen, silicon, and aluminum with contributions from iron, calcium, magnesium, and potassium (Figure 7 a). The relative

proportions of each element quantified from the survey scans (Supporting Information Table S1) after accounting for relative sensitivity factors are broadly consistent with both EDS (Figure 5) and chemical analysis results reported in Figure 6. After MFC operation there is an apparent increase in the contributions of potassium along with the appearance of a small phosphorus contribution in the survey, consistent with the use of potassium phosphate buffer in the electrolyte. No change in total iron content was found after MFC operation, however changes in the oxidation state of the iron are evident in the high resolution spectra showing the Fe 2p3/2 and 2p1/2 peaks (Figure 7 b) which may be attributed to the reduction of Fe(III) to Fe(II) by electroactive bacteria.

Chemical analysis (Figure 6, Supporting Information Figure S17) confirmed the presence of both Fe (III) and Fe (II) species which may exist as ionic species within clay minerals [45,46] and also as oxide species, further complicating the deconvolution of high-resolution spectra shown in Figure 7 c) and d). Hence, deconvolutions of the 2p3/2 peak were attempted based on characteristic multiplets for Fe (III) and Fe (II) reported in the literature[47–50], using the most prominent multiplet peaks associated to the Fe (III) and Fe (II) oxidation states. In addition, following the fitting protocol of Grosvenor et al. in reference[47], a 'pre-peak' which may also be associated to Fe(II) species and a 'surface peak,' which the authors attributed to surface effects of reduced coordination of Fe in crushed powder preparations, were found to be necessary to improve the fit. Good fits were obtained by applying this model to both PS and PS-MFC with similar values of the full width at half maximum (FWHM) and spacing between multiplets peaks, as reported in the Supporting Information Table S1 and S2. The most notable difference in the PS-MFC after MFC operation is the significant increase in the contributions of Fe(II) peaks in the region between 706-710 eV to the deconvolution.

Examining the relative peak areas for both samples yields estimates of Fe (II)/Fe(tot) of ca. 18% in PS and 40% in PS-MFC, in agreement with chemical analysis methods which suggested that the Fe(II) proportion doubled in sediments isolated after 40 days of continuous MFC operation. As XPS experiments and chemical analyses were carried out on the same samples, the lower absolute value of the estimated Fe(II) content from XPS may be explained by the overlap of multiplets associated to the two Fe oxidation states.

Discussion and Conclusions

Exoelectrogenic bacteria development has been previously demonstrated for a wide variety of soil-based inocula, suggesting a broad predominance of these bacteria in anaerobic

environments where Fe(III) and other metal oxides found in common ores may serve as alternative electron acceptors. Here we have shown that such bacteria may occupy a similar niche in marlstone which possess comparably small levels of organic matter compared to soils but are rich in clay minerals and iron. Bacteria of the genus *Geovibrio*, *Geobacter*, well known for their electroactivity [20] [51] were the main electricigens identified and are proposed to explain the observed catalytic currents as well as the bulk modifications observed in the sediment inoculum in the MFC pilots. It is likely that the exo-electrogenic bacteria present in these sediments play a role in the cycling of Fe(III) present not only as trace oxide particles but also as ions encapsulated within the clay mineral interstices. This has implications for the structural modification of marlstone by the known metabolic processes of electroactive bacteria.

The sequencing data of the interface sediment solution shows the absence of exoelectrogenic bacteria, suggesting that these bacteria are only capable of developing into extensive biofilms under artificial selection conditions conducive to MFC development. Nonetheless, once developed such biofilms were apparently capable of dramatically affecting the oxidation state of all iron present in the clay mineral, a result which was not observed in control pilots not connected to an external cathode. We speculate that observed bulk changes in sediment color and composition identified via a combination of chemical and imaging analysis are directly related to Fe(III) to Fe(II) reduction followed by subsequent reprecipitation of Fe(II) as small aggregates identified by SEM-EDS. Further research is ongoing to evaluate whether direct or indirect electron transfer processes are responsible for these bulk modifications as well as tests of a range of clay mineral organic matter and iron concentrations. Nevertheless, the results presented here strongly suggest that electroactive bacterial activity can be implicated in the modulation of marine sediment structure and composition. It demonstrates that microbial communities and clay mineral assemblages mutually interact by exerting a selection pressure on the microbial community and reducing iron contained in clay minerals such as smectite, illite and chlorite.

Declaration of Competing Interest

The authors declare that they have no known competing financial interests or personal relationships that could have appeared to influence the work reported in this paper.

Acknowledgment

This study was supported by Université de Rennes and Region Bretagne for funding under grant SAD 2076 METOX. This project has received funding from the European Union's Horizon 2020 research and innovation program under the Marie Skłodowska-Curie grant agreement No 899546. This study was supported in part by the French National Research Agency 19-CE43-0013-01 CATHOMIX). The authors thank the GeT-Biopuces platform of INSA Toulouse for the 16S rRNA gene sequencing study and Biogeosciences laboratory, University Bourgogne Franche-Comté, Dijon for XRD analysis and also the National Service of Rocks and Minerals Analysis (SARM: http://helium.crpg.cnrs-nancy.fr/SARM/) in Nancy for all the chemical analyses. We would like to thank warmly Corinne Lagrost for help XPS analyses.

Appendix A. Supplementary data

Supplementary Figures and Tables can be found in the attached file including a closer view of Col de Pré-Guittard section, paleomarine sediment (marlstone) characterization, the bioanode setup and the voltammograms of the bioanode before and after biofilm removing, additional SEM images of the biofilms developed at the surface of the bioanode, supplementary data related to the Average repartition of bacterial communities (phylum) extracted from the interface solution-sediment and color alteration recorded at the PS/MFC after development of the exoelectrogenic bacteria , supplementary Different SEM image of the PS/MFC showing the presence of biogenic new precipitate rich on iron.

References

[1] J.M. Byrne, H. Muhamadali, V.S. Coker, J. Cooper, J.R. Lloyd, Scale-up of the production of highly reactive biogenic magnetite nanoparticles using Geobacter sulfurreducens, J. R. Soc. Interface. 12 (2015). https://doi.org/10.1098/rsif.2015.0240.

[2] S.E. Childers, S. Ciufo, D.R. Lovley, Geobacter metallireducens accesses insoluble Fe(III) oxide by chemotaxis, Letters to Nature. 416 (2002) 767–769.
[3] J.D. Coates, J. Woodward, J. Allen, P. Philp, D.R. Lovley, Anaerobic degradation of polycyclic aromatic hydrocarbons and alkanes in petroleum-contaminated marine harbor sediments, Appl Environ Microbiol. 63 (1997) 3589–3593. https://doi.org/10.1128/aem.63.9.3589-3593.1997.
[4] D.R. Lovley, M.J. Baedecker, D.J. Lonergan, I.M. Cozzarelli, E.J.P. Phillips, D.I. Siegel, Oxidation of aromatic contaminants coupled to microbial iron reduction, Letters to Nature. 339 (1989) 297–300.
[5] J.C.G. Walker, Suboxic diagenesis in banded iron formations, Nature. 309 (1984) 340–342.
[6] G.M. Gadd, Metals, minerals and microbes: Geomicrobiology and bioremediation, Microbiology (N Y). 156 (2010) 609–643. https://doi.org/10.1099/mic.0.037143-0.
[7] B.E. Logan, B. Hamelers, R. Rozendal, U. Schröder, J. Keller, S. Freguia, P. Aelterman, W. Verstraete, K. Rabaey, Microbial fuel cells: Methodology and technology, Environ Sci Technol. 40 (2006) 5181–5192. https://doi.org/10.1021/es0605016.
[8] S.Z. Abbas, M. Rafatullah, N. Ismail, M.I. Syakir, A review on sediment microbial fuel cells as a new source of sustainable energy and heavy metal remediation: mechanisms and future prospective, Int J Energy Res. 41 (2017) 1242–1264. https://doi.org/10.1002/er.3706.
[9] L.M. Tender, S.A. Gray, E. Groveman, D.A. Lowy, P. Kauffman, J. Melhado, R.C. Tyce, D. Flynn, R. Petrecca, J. Dobarro, The first demonstration of a microbial fuel cell as a viable power supply: Powering a meteorological buoy, J Power Sources. 179 (2008) 571–575. https://doi.org/10.1016/j.jpowsour.2007.12.123.
[10] T. Ewing, P.T. Ha, H. Beyenal, Evaluation of long-term performance of sediment microbial fuel cells and the role of natural resources, Appl Energy. 192 (2017) 490–497. https://doi.org/10.1016/j.apenergy.2016.08.177.
[11] M. Feregrino-Rivas, B. Ramirez-Pereda, F. Estrada-Godoy, L.F. Cuesta-Zedeño, J.J. Rochín-Medina, Y.A. Bustos-Terrones, V.A. Gonzalez-Huitron, Performance of a sediment microbial fuel cell for bioenergy production: Comparison of fluvial and marine sediments|, Biomass Bioenergy. 168 (2023). https://doi.org/10.1016/j.biombioe.2022.106657.
[12] K.H. Wedepohl, Environmental Influence on the Chemical Composition of Shales and Calys, Physics and Chemistry of the Earth. (1971) 307–333.
[13] P. Corentin, J.F. Deconinck, P. Pellenard, F. Amédro, L. Bruneau, E. Chenot, B. Matrion, E. Huret, P. Landrein, Environmental and climatic controls of the clay mineralogy of Albian deposits in the Paris and Vocontian basins (France), Cretac Res. 108 (2020). https://doi.org/10.1016/j.cretres.2019.104342.
[14] J. D. Coates, J.P Phillips E, D. J Lonergan, H. Jenter, D. R. Lovley, Isolation of Geobacter Species from Diverse Sedimentary Environments, American Society for Microbiology. 62 (1996) 1531–1536.
[15] T. Philippon, F.Z. Ait-Itto, A. Monfort, F. Barrière, J.A. Behan, Fe(III) oxide microparticles modulate extracellular electron transfer in anodic biofilms dominated by bacteria of the Pelobacter genus, Bioelectrochemistry. 151 (2023). https://doi.org/10.1016/j.bioelechem.2023.108394.
[16] A. Deeke, T.H.J.A. Sleutels, H.V.M. Hamelers, C.J.N. Buisman, Capacitive bioanodes enable renewable energy storage in microbial fuel cells, Environ Sci Technol. 46 (2012) 3554–3560. https://doi.org/10.1021/es204126r.
[17] M. Picot, L. Lapinsonnière, M. Rothballer, F. Barrière, Graphite anode surface modification with controlled reduction of specific aryl diazonium salts for improved microbial fuel cells power output, Biosens Bioelectron. 28 (2011) 181–188. https://doi.org/10.1016/j.bios.2011.07.017.
[18] A. Iannaci, A. Myles, T. Flinois, J.A. Behan, F. Barrière, E.M. Scanlan, P.E. Colavita, Tailored glycosylated anode surfaces: Addressing the exoelectrogen bacterial community via

functional layers for microbial fuel cell applications, Bioelectrochemistry. 136 (2020). https://doi.org/10.1016/j.bioelechem.2020.107621.
[19] K. Fricke, F. Harnisch, U. Schröder, On the use of cyclic voltammetry for the study of anodic electron transfer in microbial fuel cells, Energy Environ Sci. 1 (2008) 144–147. https://doi.org/10.1039/b802363h.
[20] F. Caccavo, J. J.D. Coates, Geovibrio ferrireducens, a phylogenetically distinct dissimilatory Fe(III)-reducing bacterium, Arch Microbiol . 165 (1996) 370–376.
[21] P.H. Janssen, Identifying the dominant soil bacterial taxa in libraries of 16S rRNA and 16S rRNA genes, Appl Environ Microbiol. 72 (2006) 1719–1728. https://doi.org/10.1128/AEM.72.3.1719-1728.2006.
[22] D.R. Bond, D.E. Holmes, L.M. Tender, D.R. Lovley, Electrode-reducing microorganisms that harvest energy from marine sediments, Science (1979). 295 (2002) 483–485. https://doi.org/10.1126/science.1066771.
[23] D.R. Bond, D.R. Lovley, Electricity production by Geobacter sulfurreducens attached to electrodes, Appl Environ Microbiol. 69 (2003) 1548–1555. https://doi.org/10.1128/AEM.69.3.1548-1555.2003.
[24] K.C. Wrighton, P. Agbo, F. Warnecke, K.A. Weber, E.L. Brodie, T.Z. DeSantis, P. Hugenholtz, G.L. Andersen, J.D. Coates, A novel ecological role of the Firmicutes identified in thermophilic microbial fuel cells, ISME Journal. 2 (2008) 1146–1156. https://doi.org/10.1038/ismej.2008.48.
[25] D.R. Lovley, D.E. Holmes, K.P. Nevin, Dissimilatory Fe(III) and Mn(IV) reduction, Adv Microb Physiol. 49 (2004) 219–286. https://doi.org/10.1016/S0065-2911(04)49005-5.
[26] H. Rismani-Yazdi, S.M. Carver, A.D. Christy, Z. Yu, K. Bibby, J. Peccia, O.H. Tuovinen, Suppression of methanogenesis in cellulose-fed microbial fuel cells in relation to performance, metabolite formation, and microbial population, Bioresour Technol. 129 (2013) 281–288. https://doi.org/10.1016/j.biortech.2012.10.137.
[27] S. Freguia, E.H. Teh, N. Boon, K.M. Leung, J. Keller, K. Rabaey, Microbial fuel cells operating on mixed fatty acids, Bioresour Technol. 101 (2010) 1233–1238. https://doi.org/10.1016/j.biortech.2009.09.054.
[28] S.A. Haveman, R.J. DiDonato, L. Villanueva, E.S. Shelobolina, B.L. Postier, B. Xu, A. Liu, D.R. Lovley, Genome-wide gene expression patterns and growth requirements suggest that Pelobacter carbinolicus reduces Fe(III) indirectly via sulfide production, Appl Environ Microbiol. 74 (2008) 4277–4284. https://doi.org/10.1128/AEM.02901-07.
[29] D.R. Lovley, E.J.P. Phillips, D.J. Lonergan, P.K. Widman, Fe(III) and S 0 Reduction by Pelobacter carbinolicus, Appl Environ Microbiol. 61 (1995) 2132–2138. https://journals.asm.org/journal/aem.
[30] H. Richter, M. Lanthier, K.P. Nevin, D.R. Lovley, Lack of electricity production by Pelobacter carbinolicus indicates that the capacity for Fe(III) oxide reduction does not necessarily confer electron transfer ability to fuel cell anodes, Appl Environ Microbiol. 73 (2007) 5347–5353. https://doi.org/10.1128/AEM.00804-07.
[31] Z.I Kimura, S. Okabe, Hydrogenophaga electricum sp. nov., isolated from anodic biofilms of an acetate-fed microbial fuel cell, J Gen Appl Microbiol. 59 (2013) 261–266.
[32] Z.I. Kimura, S. Okabe, Acetate oxidation by syntrophic association between Geobacter sulfurreducens and a hydrogen-utilizing exoelectrogen, ISME Journal. 7 (2013) 1472–1482. https://doi.org/10.1038/ismej.2013.40.
[33] E. Ehsani, C. Dumolin, J.B.A. Arends, F.M. Kerckhof, X. Hu, P. Vandamme, N. Boon, Enriched hydrogen-oxidizing microbiomes show a high diversity of co-existing hydrogen-oxidizing bacteria, Appl Microbiol Biotechnol. 103 (2019) 8241–8253. https://doi.org/10.1007/s00253-019-10082-z.
[34] H. Wang, S. Zhou, Y. Wang, D. Kong, X. Guo, J. Zhu, W. Dong, Z. Ruan, Advenella alkanexedens sp. nov., an alkane-degrading bacterium isolated from biogas slurry samples, Int J Syst Evol Microbiol. 66 (2016) 906–911. https://doi.org/10.1099/ijsem.0.000811.

[35] S.Y. Lin, Y.C. Liu, A. Hameed, Y.H. Hsu, W.A. Lai, F.T. Shen, C.C. Young, Azospirillum fermentarium sp. nov., a nitrogen-fixing species isolated from a fermenter, Int J Syst Evol Microbiol. 63 (2013) 3762–3768. https://doi.org/10.1099/ijs.0.050872-0.
[36] S.N. Yong, S. Lim, C.L. Ho, S. Chieng, S.H. Kuan, Mechanisms of microbial-based iron reduction of clay minerals: Current understanding and latest developments, Appl Clay Sci. 228 (2022). https://doi.org/10.1016/j.clay.2022.106653.
[37] L. Zhang, G.M. Gadd, Z. Li, Microbial biomodification of clay minerals, in: Adv Appl Microbiol, Academic Press Inc., 2021: pp. 111–139. https://doi.org/10.1016/bs.aambs.2020.07.002.
[38] D.G. Zavarzina, N.I. Chistyakova, A. V. Shapkin, A. V. Savenko, T.N. Zhilina, V. V. Kevbrin, T. V. Alekseeva, A. V. Mardanov, S.N. Gavrilov, A.Y. Bychkov, Oxidative biotransformation of biotite and glauconite by alkaliphilic anaerobes: The effect of Fe oxidation on the weathering of phyllosilicates, Chem Geol. 439 (2016) 98–109. https://doi.org/10.1016/j.chemgeo.2016.06.015.
[39] G.L. Li, C.H. Zhou, S. Fiore, W.H. Yu, Interactions between microorganisms and clay minerals: New insights and broader applications, Appl Clay Sci. 177 (2019) 91–113. https://doi.org/10.1016/j.clay.2019.04.025.
[40] B. Biswas, A. Chakraborty, B. Sarkar, R. Naidu, Structural changes in smectite due to interaction with a biosurfactant-producing bacterium Pseudoxanthomonas kaohsiungensis, Appl Clay Sci. 136 (2017) 51–57. https://doi.org/10.1016/j.clay.2016.11.008.
[41] G.J. Ross, H. Kodama, Experimental alteration of a chlorite into a regularly interstratified chlorite-vermiculite by chemical oxidation, Clays Clay Miner. 24 (1976) 183–190.
[42] T. Playter, K. Konhauser, G. Owttrim, C. Hodgson, T. Warchola, A.M. Mloszewska, B. Sutherland, A. Bekker, J.P. Zonneveld, S.G. Pemberton, M. Gingras, Microbe-clay interactions as a mechanism for the preservation of organic matter and trace metal biosignatures in black shales, Chem Geol. 459 (2017) 75–90. https://doi.org/10.1016/j.chemgeo.2017.04.007.
[43] P.J.G. J.W. Stucki, Microbial reduction of iron in nontronite, (1986).
[44] B. Müller, G. Défago, Interaction between the bacterium Pseudomonas fluorescens and vermiculite: Effects on chemical, mineralogical, and mechanical properties of vermiculite, J Geophys Res Biogeosci. 111 (2006). https://doi.org/10.1029/2005JG000054.
[45] N. Finck, M.L. Schlegel, A. Bauer, Structural iron in dioctahedral and trioctahedral smectites: a polarized XAS study, Phys Chem Miner. 42 (2015) 847–859. https://doi.org/10.1007/s00269-015-0768-3.
[46] N. Finck, M.L. Schlegel, K. Dardenne, C. Adam, S. Kraft, A. Bauer, J.L. Robert, Structural iron in smectites with different charge locations, Phys Chem Miner. (2019). https://doi.org/10.1007/s00269-019-01028-y.
[47] A.P. Grosvenor, B.A. Kobe, M.C. Biesinger, N.S. McIntyre, Investigation of multiplet splitting of Fe 2p XPS spectra and bonding in iron compounds, Surface and Interface Analysis. 36 (2004) 1564–1574. https://doi.org/10.1002/sia.1984.
[48] A.K. Gupta, M. Gupta, Synthesis and surface engineering of iron oxide nanoparticles for biomedical applications, Biomaterials. 26 (2005) 3995–4021. https://doi.org/10.1016/j.biomaterials.2004.10.012.
[49] M.C. Biesinger, Accessing the robustness of adventitious carbon for charge referencing (correction) purposes in XPS analysis: Insights from a multi-user facility data review, Appl Surf Sci. 597 (2022). https://doi.org/10.1016/j.apsusc.2022.153681.
[50] N.S. McIntyre, D.G. Zetaruk, X-ray Photoelectron Spectroscopic Studies of Iron Oxides, Anal. Chem. 49 (1977) 1521–1529. https://pubs.acs.org/sharingguidelines.
[51] D.R. Lovley, Dissimilatory Fe(III) and Mn(IV) Reduction, 1991. https://journals.asm.org/journal/mr.